

Collapse of high- T_c superconductivity via ultrafast quenching of the phase coherence

F. Boschini,^{1,2,*} E. H. da Silva Neto,^{1,2,3,4} E. Razzoli,^{1,2} M. Zonno,^{1,2}
S. Peli,^{5,6} R. P. Day,^{1,2} M. Michiardi,^{1,2} M. Schneider,^{1,2} B. Zwartsenberg,^{1,2}
P. Nigge,^{1,2} R. D. Zhong,⁷ J. Schneeloch,^{7,8} G. D. Gu,⁷ S. Zhdanovich,^{1,2}
A. K. Mills,^{1,2} G. Levy,^{1,2} D. J. Jones,^{1,2} C. Giannetti,^{5,6} and A. Damascelli^{1,2,†}

¹*Department of Physics & Astronomy,*

University of British Columbia, Vancouver, BC V6T 1Z1, Canada

²*Quantum Matter Institute, University of British*

Columbia, Vancouver, BC V6T 1Z4, Canada

³*Max Planck Institute for Solid State Research,*

Heisenbergstrasse 1, D-70569 Stuttgart, Germany

⁴*Department of Physics, University of California, Davis, CA 95616, USA*

⁵*Department of Mathematics and Physics,*

Università Cattolica del Sacro Cuore, Brescia, BS I-25121, Italy

⁶*Interdisciplinary Laboratories for Advanced Materials Physics (ILAMP),*

Università Cattolica del Sacro Cuore, Brescia I-25121, Italy

⁷*Condensed Matter Physics and Materials Science,*

Brookhaven National Laboratory, Upton, NY 11973, USA

⁸*Department of Physics & Astronomy,*

Stony Brook University, Stony Brook, NY 11795-3800, USA

* boschini@phas.ubc.ca

† damascelli@phas.ubc.ca

One of the most fascinating properties of low-density condensates is the emergence of phase transitions driven solely by the fragility of the phase coherence. This intriguing physics has triggered an intense search for tools to control the rigidity of superconducting phases and investigate the collapse of superconductivity induced by phase fluctuations. Electrically-gated oxide interfaces [1, 2], ultracold Fermi atoms [3, 4] and cuprate superconductors [5, 6], which are characterized by an intrinsically small phase-stiffness, are paradigmatic examples. Here, we use ultrashort light pulses to probe and drive the phase fragility of the $\text{Bi}_2\text{Sr}_2\text{CaCu}_2\text{O}_{8+\delta}$ cuprate superconductor, up to the point of completely quenching the phase coherence without affecting the electron pairing. Time-resolved photoemission is used to track and disentangle the dynamics of phase fluctuations and charge excitations. This work demonstrates the dominant role of phase coherence in the emergence of high-temperature superconductivity and offers a new benchmark for non-equilibrium models of quantum phase transitions.

The value of the critical temperature (T_c) in a superconducting material is controlled by the interplay of two distinct phenomena: the formation of electron pairs and the onset of macroscopic phase coherence. While the pairing energy (E_p) is generally controlled by the bosonic modes that mediate the electronic interactions [7, 8], the macroscopic phase Θ depends on the robustness of the condensate against fluctuations and inhomogeneities. The energy scale relevant for phase fluctuations can be expressed via the Ginzburg-Landau theory as $\hbar\Omega_\Theta = [\hbar^2 n_S(0)a]/2m^*$, where m^* is the effective mass of the pairs, a is a characteristic length and $n_S(0)$ is the zero-temperature superfluid density. In conventional superconductors $E_p \ll \hbar\Omega_\Theta$ and therefore T_c is solely determined by the thermal charge excitations across the gap which act to reduce the number of states available for the formation of the superconducting condensate.

In cuprate superconductors, the scenario is much more complex since the small superfluid density pushes $\hbar\Omega_\Theta$ down to a value that is very close to the pairing energy [5]. The low density of the quasi-2D condensate within the Cu-O planes makes $\hbar\Omega_\Theta$ as low as ≈ 15 meV in bismuth-based copper oxides [5, 9]. Several equilibrium measurements on underdoped cuprate superconductors have reported a non-zero pairing gap up to $T \approx 1.5 \times T_c$ [10, 11] even in the absence of macroscopic phase coherence. In particular, high-resolution angle-resolved photoemission (ARPES) experiments have shown pair-breaking scattering phenomena to

emerge sharply at T_c while the pairing gap is still open, suggesting a direct connection between these latter and the onset of the phase fluctuations [12, 13]. In the same temperature range non-equilibrium optical and THz experiments have given evidence for picosecond dynamics dominated by phase fluctuations above T_c [6, 14, 15].

The idea that drives the present work is that the excitation of a high- T_c superconductor with a light pulse shorter than the internal thermalization time may be used to manipulate the density of phase fluctuations independently of the number of across-gap charge excitations. This would lead to the possibility of investigating a new transient regime that cannot be achieved in equilibrium conditions, where both phase fluctuations and charge excitations are controlled by the same temperature and thus inherently locked. Here we demonstrate this concept in the underdoped $\text{Bi}_2\text{Sr}_2\text{CaCu}_2\text{O}_{8+\delta}$ (Bi2212) superconductor ($T_c \sim 82\text{K}$). Time- and angle-resolved photoemission spectroscopy (TR-ARPES) is used to track the electronic spectral function which encodes information about the pair-breaking dynamics. We demonstrate that the pair-breaking rate Γ_p , which is experimentally [12, 13] and microscopically [16, 17] associated with the scattering off phase fluctuations, is indeed decoupled from the dynamics of the pairing gap and of the across-gap charge excitations. At the critical fluence $F_C \approx 15 \mu\text{J}/\text{cm}^2$ [18–20], the increase of Γ_p is such that superconductivity is no longer sustained. Quantitatively, we observe that the non-thermal melting of the condensate [18–23] is achieved when $\Gamma_p \approx \hbar\Omega_\Theta$.

TR-ARPES provides a direct snapshot of the one-electron removal spectral function $A(\mathbf{k}, \omega)$ [24] and its temporal evolution [25, 26] under the perturbation by an ultrashort pump pulse. The spectral function $A(\mathbf{k}, \omega)$ depends on both the electron self-energy $\Sigma(\omega) = \Sigma'(\omega) + i\Sigma''(\omega)$ and the bare energy dispersion $\epsilon_{\mathbf{k}}$:

$$A(\mathbf{k}, \omega) = -\frac{1}{\pi} \frac{\Sigma''(\omega)}{[\omega - \epsilon_{\mathbf{k}} - \Sigma'(\omega)]^2 + [\Sigma''(\omega)]^2} \quad . \quad (1)$$

For a superconductor $\Sigma(\omega)$ can be well approximated by

$$\Sigma(\omega) = -i\Gamma_s + \frac{\Delta^2}{(\omega + i\Gamma_p)} \quad , \quad (2)$$

where Δ is the superconducting gap amplitude, Γ_s is the single-particle scattering rate and Γ_p is the pair-breaking scattering rate [27]. The latter is equal to zero when the condensate is fully coherent, *i.e.* for $T \ll T_c$ at the equilibrium. This term may be interpreted as relating to the finite-lifetime of a Cooper pair induced by the scattering from phase fluctuations.

[16, 17].

First, we report the temporal evolution of the near-nodal superconducting gap. In Fig. 1a-b we display a section of the Bi2212 Fermi surface and the differential iso-energy contour mapping. The latter is obtained by the subtraction of the equilibrium iso-energy contour at 10 meV (above the Fermi level, E_F) from its counterpart obtained at 0.5 ps pump-probe delay. We focus at two points on the Fermi surface with gap amplitudes that are zero (nodal direction, black dashed line) and 15 meV (off-nodal cut, green dashed line). The data in Fig. 1b near the off-nodal region shows a clear in-gap signal that has been previously related to the quasiparticle (QP) recombination dynamics and the pairing gap closure [18, 28, 29]. In Fig. 1c we show the energy distribution curves (EDCs) at the Fermi momenta $k = k_F$ along both the nodal and off-nodal directions at two different pump-probe delays: $\tau < 0$ ps (solid lines) and $\tau = 0.5$ ps (dashed lines). Upon excitation, the QP peak is quenched and broadened, partially due to the increase in electronic temperature (Supplementary Information). However, beyond pure thermal broadening, the underlying spectral function is also modified. In Fig. 1d we show the temporal evolution of symmetrized EDCs (SEDCs), which are independent of thermal broadening [30], along the off-nodal cut at two different excitation fluences: $F < F_C$ and $F > F_C$, where F_C is the critical fluence for which the SEDCs exhibit a single peak centered at the E_F [19, 20, 31]. Under the assumption of a particle-hole symmetric spectral function near E_F , as in a superconductor [32], and neglecting matrix element effects, SEDCs allow us to explore the spectral function directly [30]. We stress that although the emergence of a single peak in SEDCs has been interpreted as a gap closure [18, 20], a careful analysis shows that a single peak in the SEDCs can be due to a gap filling [12, 13]. While a gap closure would lead to a shift of the coherent QP peaks, we observe instead a transfer of spectral weight from the coherent peaks into the gap region (Fig. 1d) indicating that the main effect of the pump excitation is a filling, not a closure, of the superconducting gap. To support our interpretation, we employ a complementary analysis based on the tomographic density of states (TDOS) method (Fig. 1e) [13]. The TDOS is obtained as the ratio between the off-nodal and nodal EDCs integrated along a momentum cut perpendicular to the Fermi surface, which approximately isolates the superconducting gap from the other spectral features, and it confirms that the primary effect of the pump excitation is to fill the gap.

We now move to a quantitative analysis of $\Sigma(\omega)$. Solid blue lines in Fig. 1d represent a fit

of the data to Eq. 1 using the self-energy from Eq. 2 (details in Supplementary Information). Figure 2a-b show the time evolution of Γ_p and Δ for the two fluences employed. Notice that the gap amplitude (Δ) does not show a significant reduction, confirming our interpretation of the data in Fig. 1. On the other hand, Γ_p considerably increases after the pump excitation, suggesting that the main cause for the gap filling is a transient loss of phase coherence of the condensate [12, 16, 17, 27].

To further support this picture we note that, in superconductors, the QP peak amplitude is directly related to the coherence of the condensate, and is quantified by the coherence factor C [33, 34]. This factor can be expressed in terms of Γ_p and Γ_s , $C(\tau) \propto \frac{1}{2}(1 + e^{-\frac{\Gamma_p(\tau)}{\Gamma_s(\tau)}})$ [34] (Supplementary Information). Accordingly, when the phase coherence of the condensate is reduced, the amplitude of the QP peak is expected to change. In Fig. 2c we compare the evolution of the spectral function amplitude (circles, obtained from the fitting procedure) and the temporal evolution of the coherence factor (dashed line). Remarkably, the dynamics of both the QP peak amplitude and C agree, supporting our previous assertions and explaining thoroughly the relation between the nodal QP peak and the superfluid density reported in Ref. [31].

The possibility of accessing the evolution of Γ_p in the time-domain provides pivotal information about the intrinsic dynamics of the condensate formation in cuprates. Figure 3a,b show that the Γ_p relaxation dynamics for $F < F_C$ is completely decoupled from that of the gap amplitude and of the above-gap charge excitations. In particular, in Figure 3b we compare the temporal evolution of Γ_p (blue) with the dynamics of the superconducting gap (black) and of the charge excitations (green), as obtained by integrating the off-nodal pump-induced charge population in the above-gap (15-70 meV) energy window shown in the inset of Fig. 3b. While the temporal evolution of the above gap excitations and of the gap amplitude are locked, as expected for a superconductor in quasi-equilibrium conditions, Γ_p relaxes much faster with a relaxation rate $\tau_\Theta \approx 1$ ps, a value of the order of the phase-correlation time extracted from high-frequency conductivity and related to the motion of topological defects [6].

Microscopically, the transient increase of phase fluctuations can be rationalized as a cascade process triggered by the optical pump, which initially breaks the electronic pairs and promotes hot QPs to energies well above E_F . During their decay, the non-thermal QP population can either couple directly to phase excitations or scatter off high-energy

bosonic excitations on a time scale of tens (spin fluctuations) to hundreds (optical phonons) of femtoseconds [35, 36]. The subsequent absorption of these bosons can eventually break additional Cooper pairs. Simultaneously, any pair recombination process must emit a gap-energy boson in order to satisfy energy conservation, as described by the Rothwarf-Taylor equations [23]. As a result, after a few hundreds of femtoseconds the initial excitation is converted into a non-thermal bosonic population. We speculate that these highly energetic bosons, coupled to the fermionic bath, can interact, even indirectly, with the macroscopic condensate. They can thus be considered as a possible source of the excess phase fluctuations which introduce a finite lifetime to the Cooper pairs. This picture is corroborated by the observation that the maximum change of Γ_P (Fig. 3a) is observed approximately 500 fs after the pump excitation. This value is compatible with the build-up time observed via time-resolved optical spectroscopy and it has been attributed to the time necessary for the growth of the non-thermal gap-energy bosonic population [23].

All these observations clearly imply that the pair breaking processes related to the loss of coherence of the condensate can be decoupled from the charge excitations on the picosecond timescale. In this transient state, the condensate becomes more fragile, despite an almost unaffected pairing strength. This result has important consequences for establishing the nature of the instability of the macroscopic condensate at larger excitation fluences. Both time-resolved optical [21–23, 37, 38] and photoemission [18–20, 28, 31, 39] experiments have shown the collapse of superconductivity and the complete quench of the coherence factor for pump fluence excitations ranging from 14 to 70 $\mu\text{J}/\text{cm}^2$. Our data demonstrate that at $F \geq 15 \mu\text{J}/\text{cm}^2$ the non-equilibrium pair breaking rate is of the order of the energy scale relevant to phase fluctuations, i.e. $\Gamma_p \approx \hbar\Omega_\Theta \approx 15 \text{ meV}$ (Fig. 2b), similar to the pairing energy, which corresponds to a lifetime of the Cooper pairs of ≈ 40 fs. Figure 3c provides a pictorial illustration of the dynamics of the superconductor-to-normal state phase transition driven by the loss of phase coherence.

This work impacts in many ways the current knowledge of the superconducting phase transition in cuprates and opens new interesting possibilities. The TR-ARPES data presented here constitute direct evidence that the phase coherence controls the condensate formation in high- T_C superconductors, while the temperature-driven pairing plays a subordinate role [5]. Indeed, our results demonstrate that the recovery of phase coherence is the primary and fastest mechanism that leads to the onset of superconductivity (see Fig. 3a).

Moreover, the ability to melt the condensate without altering the gap size or increasing considerably the charge temperature provides a new platform for investigating the hierarchy of the pairing and phase coherence throughout the cuprate phase diagram and in the vicinity of the putative quantum critical points. Finally, further investigation and the development of selective excitation schemes would help clarifying the microscopic mechanisms responsible for the increase of phase instability. The way fermions interact with phase modes and how gap-energy bosons interact with the pair condensate, up to the point of turning it into a plasma of incoherent excitations, still remains as an open and intriguing issue.

METHODS

Our TR-ARPES system is based on a Ti:Sapphire laser (VitesseDuo + RegA 9000 by Coherent) delivering 800 nm pulses (1.55 eV) with a 180-fs pulse duration, 250-kHz repetition rate. The output beam is split: a portion is used as the pump beam while the remaining part generates its fourth-harmonic, *i.e.* 200 nm (6.2 eV). The 6.2-eV is generated through a cascade of nonlinear processes. The probe (6.2 eV) and the pump (1.55 eV) beams were both vertically (s) polarized. The ARPES measurements are conducted in ultra-high-vacuum with a base pressure lower than $3 \cdot 10^{-11}$ Torr, at a base temperature of 6 K, and the angle and energy of the photoelectrons are resolved using a SPECS Phoibos 150 electron analyzer. The momentum, energy and temporal resolutions of the system are $<0.0002 \text{ nm}^{-1}$, 19 meV and 250 fs, respectively, referenced from polycrystalline gold. Incident pump fluences indicated as $F < F_C$ and $F > F_C$ correspond to $8 \mu\text{J}/\text{cm}^2$ and $30 \mu\text{J}/\text{cm}^2$, respectively.

ACKNOWLEDGMENTS

We thank L. Benfatto, A. Chubukov and M. Franz for useful and fruitful discussions. C.G. acknowledge financial support from MIUR through the PRIN 2015 Programme (Prot. 2015C5SEJJ001) and from Università Cattolica del Sacro Cuore through D.1, D.2.2 and D.3.1 grants. This research was undertaken thanks in part to funding from the Max Planck-UBC Centre for Quantum Materials and the Canada First Research Excellence Fund, Quantum Materials and Future Technologies Program. The work at UBC was supported by the Killam, Alfred P. Sloan, and Natural Sciences and Engineering Research Council of

Canadas (NSERCs) Steacie Memorial Fellowships (A.D.), the Alexander von Humboldt Fellowship (A.D.), the Canada Research Chairs Program (A.D.), NSERC, Canada Foundation for Innovation (CFI), CIFAR Quantum Materials and CIFAR Global Scholars (E.H.d.S.N.). E.R. acknowledges support from the Swiss National Science Foundation (SNSF) grant no. P300P2-164649. GDG is supported by the Office of Basic Energy Sciences, Division of Materials Sciences and Engineering, U.S. Department of Energy under contract No. DE-AC02-98CH10886. JS and RDZ are supported by the Center for Emergent Superconductivity, an Energy Frontier Research Center funded by the U.S. Department of Energy, Office of Science.

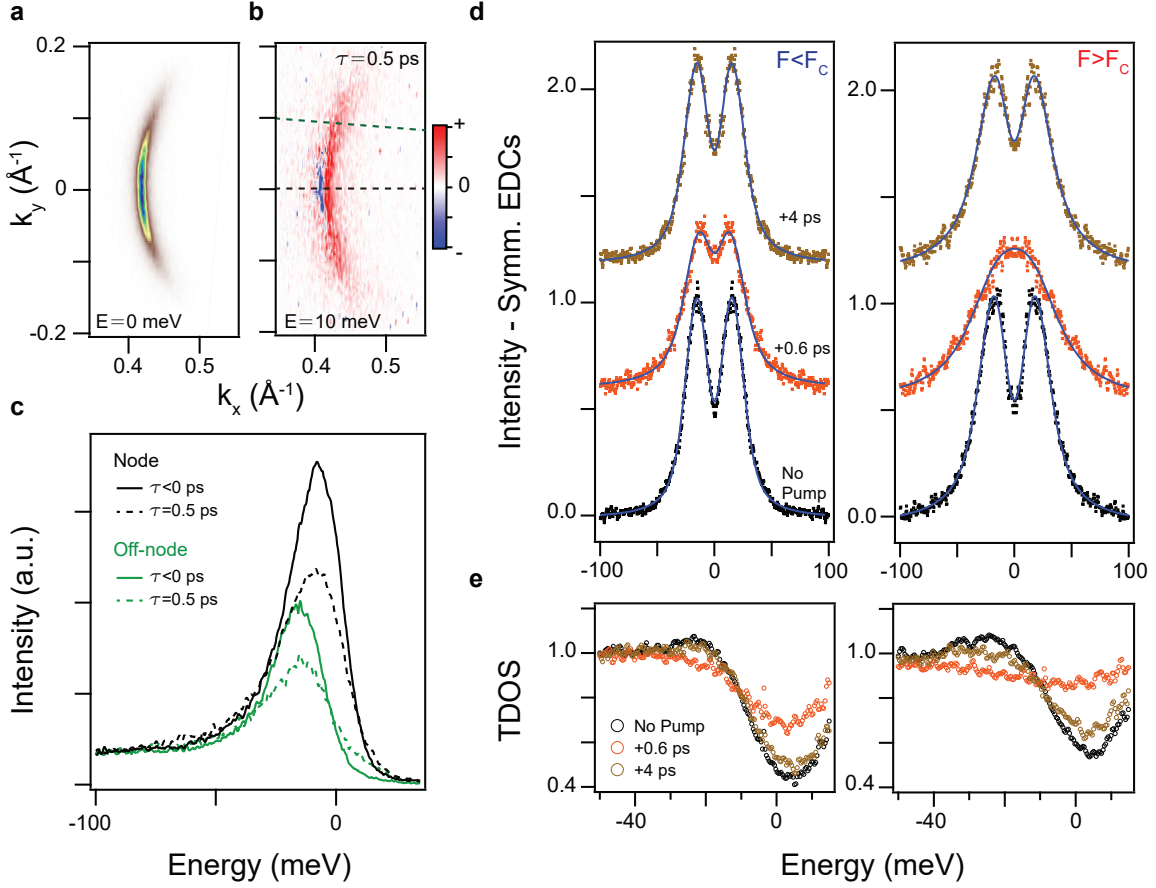


FIG. 1. **a-b** Equilibrium Fermi Surface mapping and differential (Pump_{on}-Pump_{off}) iso-energy contour mapping at 10 meV above the Fermi level E_F , 0.5 ps pump-probe delay. The integration energy range is 10 meV and k_x is aligned along the Γ -Y direction. The dashed black and green lines in b define the nodal and off-nodal cuts investigated in the present work. **c** Energy distribution curves (EDCs) at $k = k_F$, $F < F_C$ fluence, along the nodal direction (black lines) and the off-nodal cut (green lines): solid lines $\tau < 0$ ps pump-probe delay, dashed lines $\tau = 0.5$ ps pump-probe delay. **d** Symmetrized EDCs (SEDCs) at $k = k_F$, off-nodal cut. SEDCs have been fit using the self-energy from Eq. 2 (blue lines). Additional details on the fitting procedure and analysis are described in the Supplementary Information. **e** Tomographic density of states (TDOS) at different pump-probe delays along the off-nodal cut. The minimum of the TDOS curves is not centered at a zero energy due to the energy resolution broadening effect.

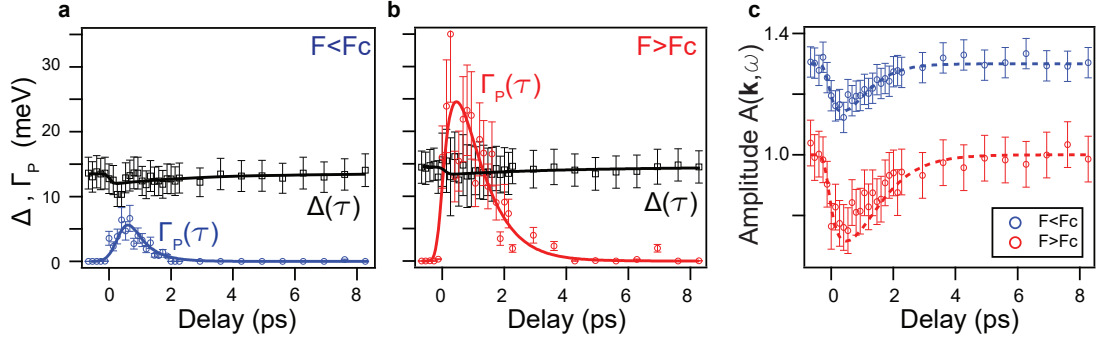


FIG. 2. **a-b** Ultrafast dynamics of Δ and the pair-breaking term, Γ_p , resulting from the fit of SEDCs shown in Fig. 1d. Pump excitation fluences are defined as $F < F_C$, panel a, and $F > F_C$, panel b, where $F_C \approx 15 \mu\text{J}/\text{cm}^2$. Solid lines derive from a phenomenological fit by a bi-exponential function convolved with a Gaussian accounting for the temporal resolution. **c** Temporal evolution of the amplitude of the spectral function (normalized at $\tau < 0$ ps, circles) and of C as defined in the main text (dashed lines).

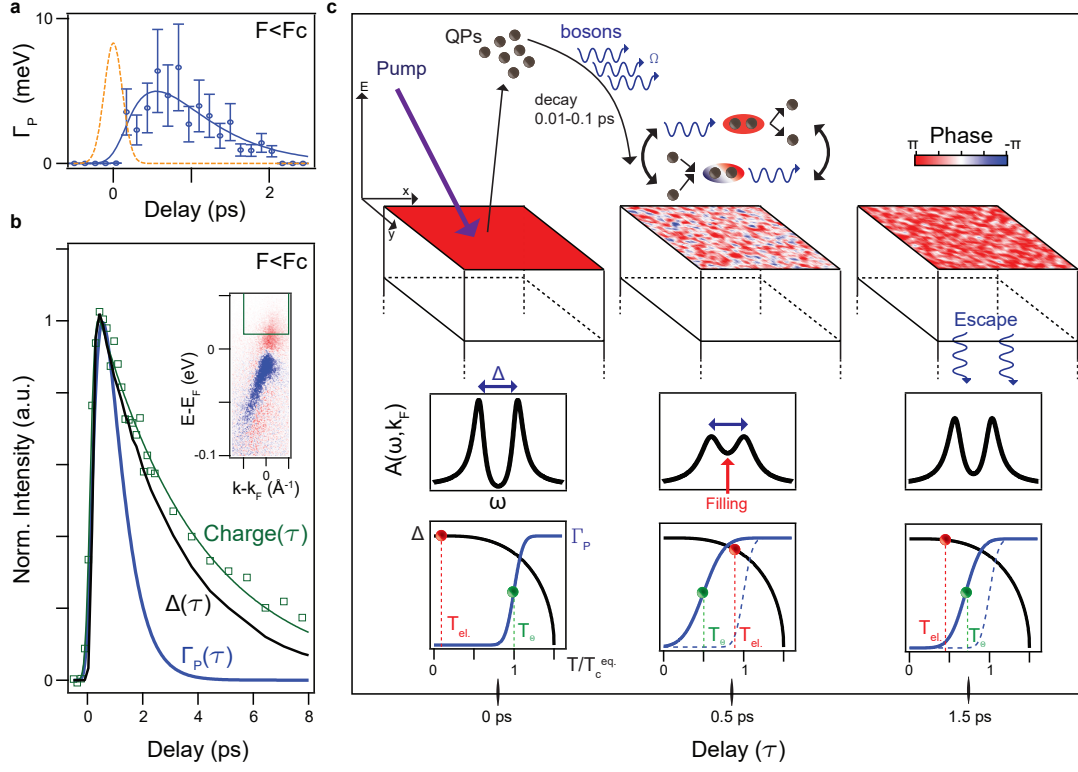


FIG. 3. **a** Γ_p dynamics at $F < F_C$ (blue circles while the blue line is the phenomenological fit curve described in Fig. 2) compared to the pump-probe cross-correlation (orange dashed line). **b** Comparison of the normalized dynamics of the phenomenological fit of Γ_p (blue line), gap amplitude (black line) and the charge dynamics (green squares and line) at $F < F_C$. The charge dynamics is extracted by integrating the off-nodal pump-induced population in the above-gap 15-70 meV energy window (inset). **c** Pictorial sketch of the transient collapse of the condensate: a non-equilibrium bosonic population induces phase fluctuations leading to a gap filling and a modification of the temperature where the phase coherence is set independently to the charge dynamics. Top panels show a cartoon of the energetics of the process and the related real space condensate phase coherence; mid panels display the spectral function at $k = k_F$ when phase fluctuations are induced; bottom panels show the pairing strength (Δ , gap amplitude, black line) as the function of the electronic temperature ($T_{el.}$, red spheres and dashed lines) and the pair-breaking scattering rate (Γ_p , blue line) which is related to the onset of the phase coherence $T_\Theta \approx \hbar\Omega_\Theta/k_B$ (green spheres and dashed lines).

Supplementary Information

I. EQUILIBRIUM DATA ANALYSIS

Here we accurately describe how angle-resolved photoemission (ARPES) data presented in the main text have been analyzed. In Fig. S1 we show raw data at the equilibrium, $T=6$ K base temperature, s-polarized 6.2-eV light. Figure S1a-b display the band mapping along the nodal direction ($\varphi=45^\circ$) and an off-nodal cut ($\varphi=36^\circ$), respectively. The Fermi surface mapping (15 meV integration range) is shown in Fig. S1c. Three momentum cuts have been acquired: $\varphi=45^\circ$ nodal cut (black line), $\varphi=40^\circ$ near-nodal cut (green line) and $\varphi=36^\circ$ off-nodal cut (red line).

The photoemission signal can be written as [24]

$$I(k, \omega) = A(k, \omega) \cdot |M|^2 \cdot f(\omega), \quad (3)$$

where $A(k, \omega)$ is the one-electron removal spectral function, $|M|^2$ the matrix element and $f(\omega)$ an electronic distribution. The spectral function $A(k, \omega)$ can be expressed in terms of the self-energy ($\Sigma = \Sigma' + i\Sigma''$) to account for many-body interactions:

$$A(k, \omega) = -\frac{A_{QP}^k}{\pi} \frac{\Sigma''(k, \omega)}{[\omega - \epsilon_k - \Sigma'(k, \omega)]^2 + [\Sigma''(k, \omega)]^2}, \quad (4)$$

where ϵ_k is the bare energy dispersion, A_{QP}^k is the coherent amplitude, $\Sigma'(k, \omega)$ and $\Sigma''(k, \omega)$ describe the band dispersion renormalization and the quasiparticle (QP) lifetime, respectively.

For a superconductor, in the BCS framework, the electron self-energy can be written as [17, 27]

$$\Sigma(\omega) = -i\Gamma_s + \frac{\Delta^2}{\omega + \epsilon_k + i\Gamma_p}, \quad (5)$$

where Δ is the superconducting gap amplitude, Γ_s the single-particle scattering rate and Γ_p the pair-breaking scattering rate, *i.e.* the inverse lifetime of the Copper pairs. Note that here we are assuming a momentum-independent self-energy and that the $\Gamma_{s,p}$ terms are assumed to be constant in energy. This assumption works well in a limited energy window of few tens of meV around the Fermi level (E_F). We remark that equation (5) successfully captures the properties of the superconducting phase in d-wave high- T_C superconductors when the employed momentum cut allows to define well a gap amplitude (radial cut to the

(π,π) -centered hole-pocket) [12].

ARPES allows a direct access the one-electron removal spectral function. In fact, under

TABLE I. Parameters extracted from the fitting procedure shown in Fig. S2.

Cut φ (deg)	Δ (meV)	Γ_s (meV)	Γ_p (meV)
45	0	10.9 ± 0.2	0
40	6 ± 0.4	10.2 ± 0.4	0
36	14.7 ± 0.2	11.8 ± 0.2	0

the assumption of a particle-hole symmetric spectral function at the Fermi momentum $k=k_F$ [32], the symmetrized energy distribution curves (SEDCs) do not depend on the electronic temperature [30], *i.e.* $f(\omega)$. Moreover, assuming a constant matrix element, $\text{SEDC}(\omega) \propto A(k_F, \omega) * R(\omega)$, where $R(\omega)$ is a Gaussian function accounting for the energy resolution. Equilibrium SEDCs along the three momentum cuts are shown in Fig. S2. The blue lines are the curves resulting from the fitting procedure using Eqs. (4)-(5). In Table I we list extracted parameters. In agreement with Kondo et al. [27], $\Gamma_p=0$ at $T \ll T_C$ while Γ_s is finite for every temperature and almost momentum independent. The gap amplitude is consistent with what has already been reported [29].

II. TEMPORAL EVOLUTION OF THE SYMMETRIZED ENERGY DISTRIBUTION CURVES

In Fig. 2 of the main text we have shown the temporal evolution of the pairing gap amplitude and the pair-breaking scattering term. Here below we discuss how the pump excitation transiently modifies the spectral function and we provide details about the fitting procedure of the transient SEDCs. Generally, several effects can modify the out-of-equilibrium photoemission signal. To a first approximation, a hole is present in the occupied manifold after an optical transition induced by the pump. Naturally, this results in an increase of the single-particle scattering rate, Γ_s , due to the availability of novel scattering channels and consequently affects $\Sigma(\omega)$ [40]. Additionally, pump-triggered coherent phonons may induce a deformation potential, which modifies the bare energy dispersion [41]. For super-

conductors, any modification of the phase coherence and/or pairing strength will also affect $A(k, \omega)$. Thus, upon the pump excitation, Γ_p , Γ_s and Δ parameters contained in eq. (5) and the electronic distribution $f(\omega)$ can vary. The coherent amplitude of the spectral function, A_{QP} , is an additional parameter possibly evolving. The concurrent temporal evolution of all three parameters inside Σ (Γ_p , Γ_s and Δ) and of the spectral function amplitude A_{QP} , may affect the stability of the SEDCs fit. The problem is overcome by noting that the SEDCs along the nodal cut depend only on Γ_s and A_{QP} (the node is gapless). In Fig. S3a we show the SEDCs along the nodal cut at three different pump-probe delays (solid blue lines display the quality of the fit). The extracted nodal Γ_s dynamics is displayed in Fig. S3b and it is fit well by a single exponential decay function (red solid line). Static ARPES experiments have shown that Γ_s is isotropic in momentum, at least around the nodal point, within a wide temperature range [12]. Thus, we expect similar Γ_s dynamics along the nodal and the off-nodal cuts. Substituting and holding the nodal Γ_s dynamics in the off-nodal SEDCs fit procedure, we can extract the dynamics of both Γ_p and Δ for the off-nodal cut, as shown in the main text. The quality of the off-nodal SEDCs fit is displayed in Fig. S3c (blue lines). Here below we discuss the importance of the Γ_p term in describing the evolution of the SEDCs along the off-nodal cut. When SEDCs are fit imposing $\Gamma_p(\tau)=0$, the gap shows an almost complete closure at $F > F_C$ pump fluence (*i.e.*, when a single peak appears in the SEDCs, see Fig. S4a), as reported in several works [18, 20]. Note that for measurements performed at $F > F_C$ fluence, the equilibrium value of Γ_s is almost two times larger than the one obtained at $F < F_C$. This is due to the fact that we performed measurements at $F > F_C$ in a different position of the sample where surface defects and inhomogeneities might have affected Γ_s adding a constant offset (electron-impurity scattering is a possible explanation). We show that the maximum transient value of Γ_s extracted along the off-nodal direction (when $\Gamma_p(\tau)=0$) is two times larger than the equilibrium one. We point out that: (i) the Γ_s dynamics extracted along the nodal direction is different than the one along the off-nodal cut with $\Gamma_p(\tau)=0$ (inset of Fig. S4a) and (ii) if $\Gamma_p(\tau)=0$ is imposed in the fit of the SEDCs along the off-nodal cut, the spectral function amplitude does not change, in contradiction to the observed quenching of the QP peak along the nodal direction. Different Γ_s dynamics at different momenta disagree with our previous discussion. Additionally, we stress that the transient self-energy extracted from the fit of SEDCs at $k=k_F$ can be used to calculate the momentum distribution curves (MDCs) and compare them with experimental ones

(Fig. S4b). The agreement is remarkable only when $\Gamma_p(\tau)$ is free to change while, with $\Gamma_p(\tau)=0$, the MDC width at 0.6 ps delay (green dashed curve) does not match with what observed experimentally due to the large variation of the single-particle scattering term Γ_s .

III. Γ_p DYNAMICS: TEMPORAL AND MOMENTUM DEPENDENCE

In the main text we have extensively discussed the importance of the pair-breaking term Γ_p in describing the temporal evolution of the spectral function. Moreover, we have addressed a transient bosonic population as the most probable mediator of the pair-breaking events. In Fig. S5 we show Γ_p extracted at $F > F_C$ fluence along two off-nodal cuts: $\varphi=36^\circ$ (the same shown in the main text) and $\varphi=40^\circ$. While for the former cut, two peaks can be well identified in the equilibrium SEDCs, for the latter cut our energy resolution prevents us from directly observing the two peaks (see Fig. S2). The extraction of the Γ_p term at $\varphi=40^\circ$ is consequently based on the evolution of the SEDCs width. The two Γ_p dynamics are compared to the dynamics of the photoemission intensity 0.1 eV above E_F (0.1-0.12 eV range) along the nodal direction, a sort of pump-probe cross-correlation (XC) measurement. Results shown in Fig. S5 suggest that: (i) Γ_p value and dynamics are isotropic in the near nodal region; (ii) the maximum of Γ_p is clearly delayed with respect to the pump arrival and presents a sizable rise-time. This rise time, not limited by our temporal resolution, is around 500 fs, in agreement with the value reported in the main text for $F < F_C$ and with the picture of a transient bosonic population excited by non-equilibrium QPs [23].

IV. TRANSIENT ELECTRONIC TEMPERATURE

We show here the temporal evolution of the electronic temperature in order to additionally prove that the transient enhancement of the pair-breaking scattering phenomena is not just a pure thermal effect. We can extract an approximate transient electronic temperature T_e by fitting the EDC at $k=k_F$ along the nodal direction. The fitting function $Fit(\omega)$ is defined as the product between the nodal spectral function at $k=k_F$ with amplitude A_{QP} and the

Fermi Dirac distribution $f_{FD}(\omega) = \frac{1}{e^{\frac{\omega}{k_B T_e}} + 1}$ and it can be expressed as:

$$Fit(\omega) = \left[\frac{A_{QP}}{\pi} \frac{\Gamma_s}{\omega^2 + \Gamma_s^2} \cdot f_{FD}(\omega) \right] * R(\omega). \quad (6)$$

It is clear that both Γ_s and T_e can influence the temporal evolution of the nodal line-shape. In Fig. S6a we show simulated nodal EDCs using eq. (6) by changing Γ_s and T_e parameters (19 meV energy resolution). If Γ_s dynamics was not included in the electronic temperature extraction procedure, T_e would be overestimated. Moreover, a change in Γ_s results in an apparent depletion even above the Fermi level, as observed in the differential Fermi Surface shown in Fig. 1b in the main text. We stress that an evolution of A_{QP} , even if not considered in Fig. S6a, may also influence the T_e extraction. In Fig. S6b we show the extracted temporal evolution of T_e for both the employed fluences. While for $F > F_C$ fluence the maximum electronic temperature is $T_e^{max} > T_C$, for $F < F_C$ $T_e^{max} \approx T_C/2$. This is an additional evidence that the transient Γ_p is not due to a pure thermal effect [12] but has a deeper physical meaning. Additionally, static ARPES experiments [12, 13] have shown that the superconducting gap amplitude follows a BCS-like temperature dependence with a closing temperature $T_{close} \approx 140$ K. Thus, even for the $F > F_C$ fluence, where $T_e^{max} \approx 110$ K $> T_C$, we expect a gap quenching of around 30%, consistently to what reported in the main text.

V. COHERENT FACTOR: QUASIPARTICLE PEAK AMPLITUDE

Figure S7 displays the differential ARPES maps (Pump – NoPump) at 0.5 ps delay, along the nodal and off-nodal directions for $F > F_C$ incidence fluence. A linear color scale is chosen in order to highlight that the stronger transient modification happens at the QP peak. In the main text we stress the relation between the QP peak amplitude and the phase coherence of the condensate. Moreover, we show that the reduction of the QP peak amplitude is well described by a variation of the coherence of the condensate in tandem with the QP scattering rate. Below we show how the coherence factor C can be written in terms of Γ_p , the inverse of the Cooper pair lifetime.

The coherent factor can be written as [33, 34, 42]

$$C = \frac{1}{2} \left(1 + \frac{\Delta_k \Delta_{k'}}{E_k E_{k'}} \right), \quad (7)$$

where Δ_k is the d-wave complex order parameter, $\Delta_k = |\Delta_k|e^{i\phi_k}$ and $E_{k,k'}$ are the initial and final energy of the scattered QP. Thus, $C = \frac{1}{2}(1 + |\Delta_k||\Delta_{k'}|\frac{e^{i(\phi_k+\phi_{k'})}}{E_k E_{k'}})$. QP interference experiments have shown that, within the octec model, QPs scattering events happen between points of the Brillouin zone with similar gap amplitude [33, 43]. Furthermore, the QP peak observed in ARPES is localized at energies $E_k \approx |\Delta_k|$, thus

$$C \approx \frac{1}{2}(1 + e^{i\phi}), \quad (8)$$

where $\phi = \phi_k + \phi_{k'}$. Depending on the initial and the final scattering states, $\phi = 0, \pi$. We stress that phase gradients influence the scattering in a similar way as magnetic impurities, enhancing the scattering rate between regions having the same order parameter sign, *i.e.* $\phi = 0$ [33].

In a light-scattering experiment, like ARPES, the coherent factor is dictated by the ensemble average of the phase: $\langle C \rangle \approx \frac{1}{2}(1 + \langle e^{i\phi} \rangle)$. Following the work of Hinton et al. [34], we write the spatial ensemble average of the phase as $\langle e^{i\phi} \rangle = e^{-\frac{\tau_s}{\tau_p}}$, where τ_s is the QP lifetime in the fully incoherent regime and τ_p is the phase-correlation time. This observation allows us to finally express the temporal evolution of the coherence factor in terms of Γ_s and Γ_p :

$$\langle C(\tau) \rangle = \frac{1}{2}(1 + e^{-\frac{\Gamma_p(\tau)}{\Gamma_s(\tau)}}). \quad (9)$$

This clearly shows that pair-breaking events reduce $\langle C \rangle$.

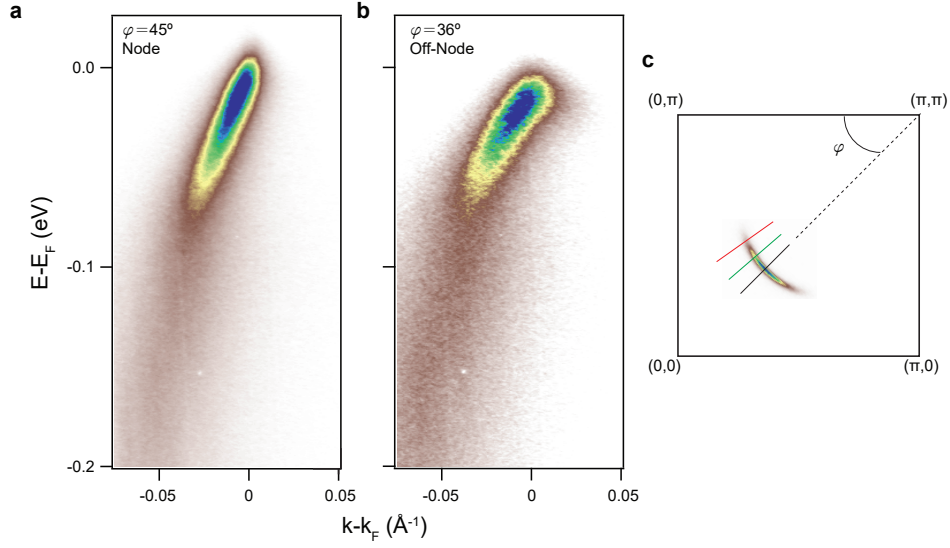


FIG. S1. **a-b** Band mapping at the equilibrium with s-polarized 6.2 eV light, base temperature 6 K, along the nodal direction ($\varphi=45^\circ$) and an off-nodal cut ($\varphi=36^\circ$), respectively. **c** Fermi surface mapping in a quadrant of the Brillouin zone. The sample was aligned along the $\Gamma - Y$ direction. The φ angle is defined with respect to the $(0,\pi)$ - (π,π) direction. The three colored lines indicate the three measured momentum cuts: the nodal cut (black), a near-nodal cut (green) and an off-nodal cut (red).

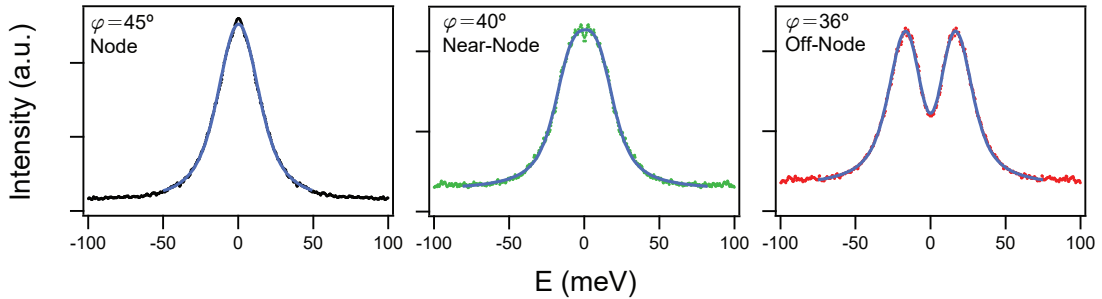


FIG. S2. Equilibrium SEDCs for the three measured momentum cuts. The blue lines show the fit resulting from Eqs. (4)-(5).

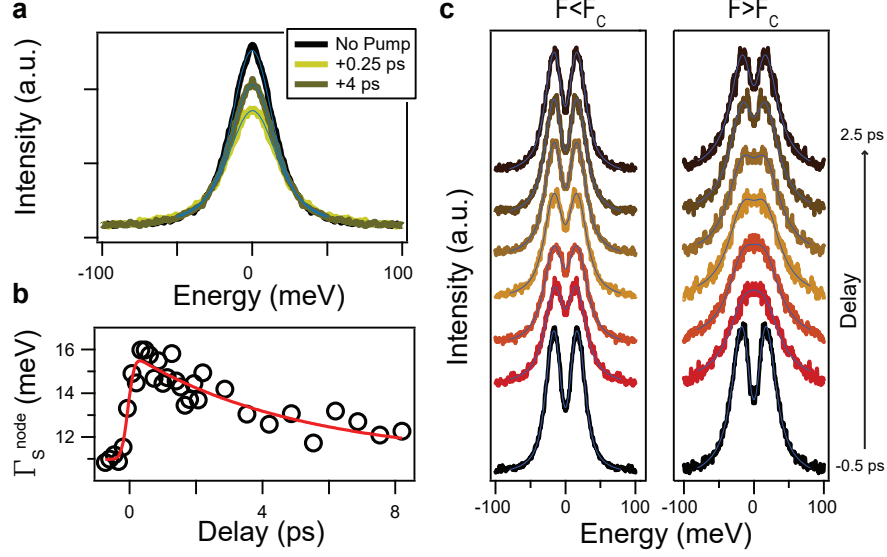


FIG. S3. **a** SEDCs along the nodal direction at three different delays ($F < F_C$ fluence). **b** Γ_s dynamics extracted along the nodal direction ($F < F_C$). The red line represents the fit with a single exponential decay function convolved with a Gaussian. **c** SEDCs along the off-nodal cut at different pump-probe delays for the two employed pump fluences, $F < F_C$ and $F > F_C$.

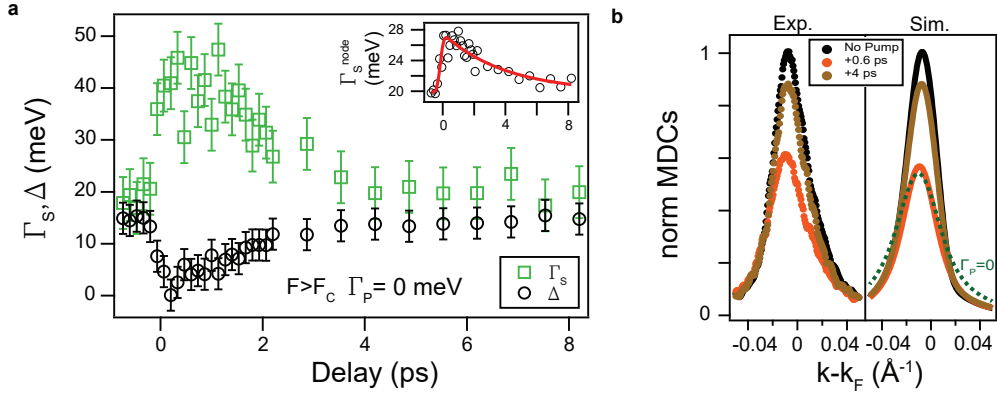


FIG. S4. **a** Γ_s and Δ dynamics extracted along the off-nodal cut by imposing $\Gamma_p(\tau)=0$. The inset shows the Γ_s dynamics extracted along the nodal direction at $F > F_C$ fluence. **b** Comparison between experimental and simulated MDCs, off-nodal cut, -20 meV binding energy. The dashed green line shows the simulated MDC at +0.6 ps pump-probe delay when $\Gamma_p(\tau)=0$ is imposed.

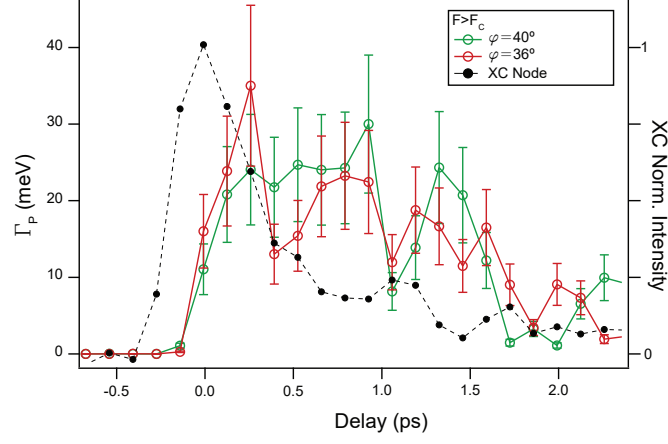


FIG. S5. Γ_p dynamics extracted along the near-nodal direction ($\varphi=40^\circ$, green line) and the off-nodal direction ($\varphi=36^\circ$, red line) for $F > F_C$ fluence. The black dashed line is the temporal evolution of the population extracted 0.1 eV above E_F along the nodal direction as a reference for the zero pump-probe delay and the temporal resolution.

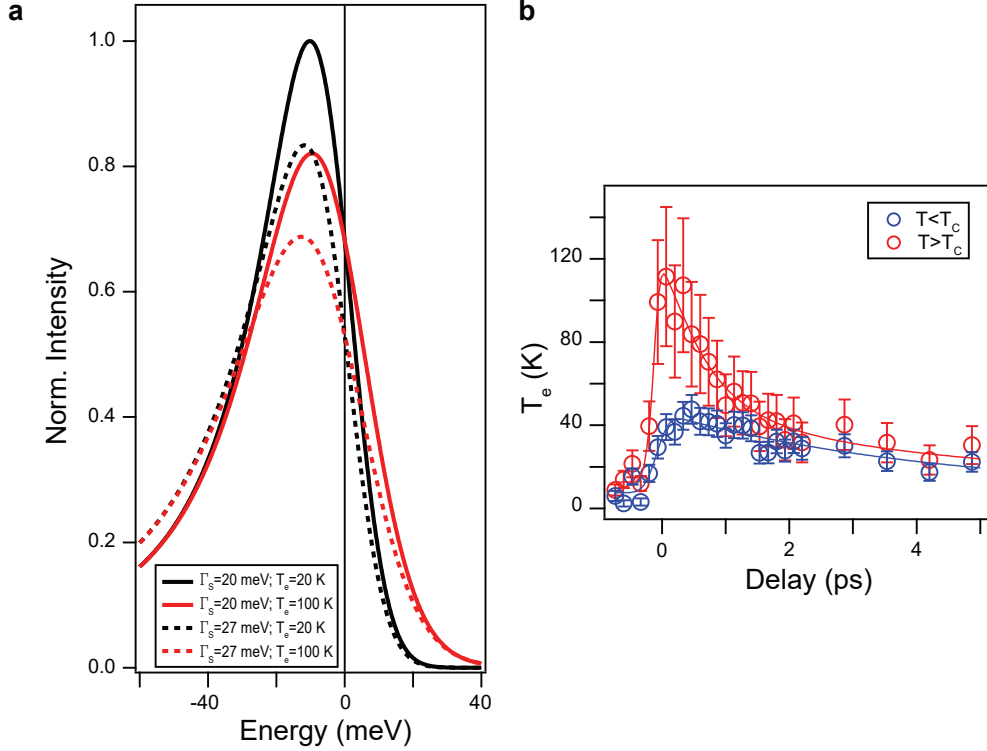


FIG. S6. **a** Simulated EDCs at $k = k_F$ along the nodal direction as function of Γ_s and T_e parameters. **b** Extracted dynamics of the electronic temperature T_e for both $F < F_C$ and $F > F_C$.

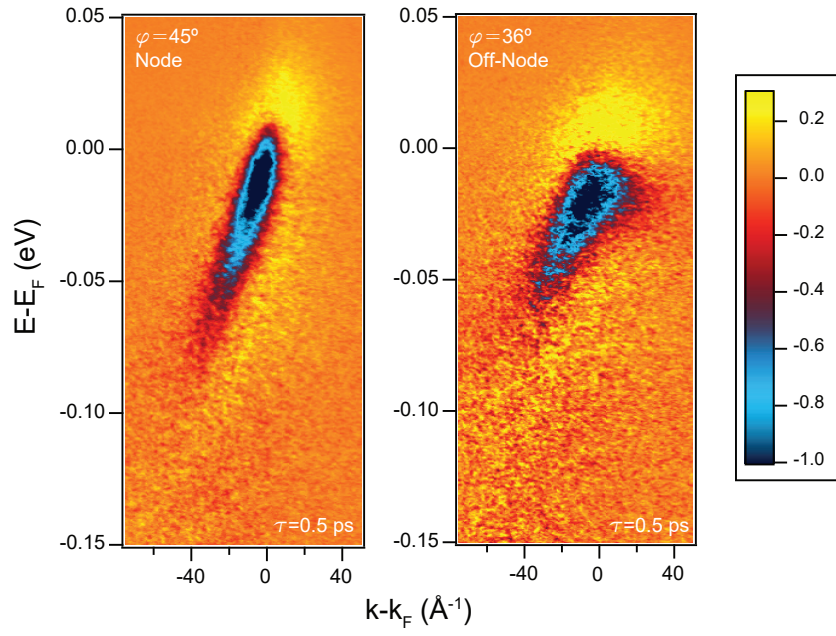


FIG. S7. Differential ARPES maps (Pump $_{\tau=0.5ps}$ -NoPump) along the nodal and the off-nodal cuts.

-
- [1] A. D. Caviglia, S. Gariglio, N. Reyren, D. Jaccard, T. Schneider, M. Gabay, S. Thiel, G. Hammerl, J. Mannhart, and J.-M. Triscone, *Nature* **456**, 624 (2008).
- [2] H. Y. Hwang, Y. Iwasa, M. Kawasaki, B. Keimer, N. Nagaosa, and Y. Tokura, *Nat Mater* **11**, 103 (2012).
- [3] C. Regal and D. Jin (Academic Press, 2007) pp. 1 – 79.
- [4] J. P. Gaebler, J. T. Stewart, T. E. Drake, D. S. Jin, A. Perali, P. Pieri, and G. C. Strinati, *Nat. Physics* **6**, 569 (2010).
- [5] V. J. Emery and S. A. Kivelson, *Nature* **374**, 434 (1995).
- [6] J. Corson, R. Mallozzi, J. Orenstein, J. N. Eckstein, and I. Bozovic, *Nature* **398**, 221 (1999).
- [7] S. Johnston, W. S. Lee, Y. Chen, E. A. Nowadnick, B. Moritz, Z.-X. Shen, and T. P. Devereaux, *Advances in Condensed Matter Physics* **2010**, 968304.
- [8] V. Kordyuk, A.A.and Zabolotnyy, D. Evtushinsky, D. Inosov, T. Kim, B. Büchner, and S. Borisenko, *The European Physical Journal Special Topics* **188**, 153 (2010).
- [9] L. Benfatto, S. Caprara, C. Castellani, A. Paramekanti, and M. Randeria, *Phys. Rev. B* **63**, 174513 (2001).
- [10] Y. Wang, Z. A. Xu, T. Kakeshita, S. Uchida, S. Ono, Y. Ando, and N. P. Ong, *Phys. Rev. B* **64**, 224519 (2001).
- [11] L. Li, Y. Wang, S. Komiya, S. Ono, Y. Ando, G. D. Gu, and N. P. Ong, *Phys. Rev. B* **81**, 054510 (2010).
- [12] T. Kondo, W. Malaeb, Y. Ishida, T. Sasagawa, H. Sakamoto, T. Takeuchi, T. Tohyama, and S. Shin, *Nature Commun.* **6**, 7699 (2015).
- [13] T. J. Reber, N. C. Plumb, Z. Sun, Y. Cao, Q. Wang, K. McElroy, H. Iwasawa, M. Arita, J. S. Wen, Z. J. Xu, G. Gu, H. Yoshida, Y. adn Eisaki, Y. Aiura, and D. S. Dessau, *Nat Phys* **8**, 606 (2012).
- [14] I. Madan, T. Kurosawa, Y. Toda, M. Oda, T. Mertelj, P. Kusar, and D. Mihailovic, *Scientific Reports* **4**, 5656 (2014).
- [15] L. Perfetti, B. Sciolla, G. Birolì, C. J. van der Beek, C. Piovera, M. Wolf, and T. Kampfrath, *Phys. Rev. Lett.* **114**, 067003 (2015).
- [16] M. Franz and A. J. Millis, *Phys. Rev. B* **58**, 14572 (1998).

- [17] H.-J. Kwon and A. T. Dorsey, *Phys. Rev. B* **59**, 6438 (1999).
- [18] C. L. Smallwood, J. P. Hinton, C. Jozwiak, W. Zhang, J. D. Koralek, H. Eisaki, D.-H. Lee, J. Orenstein, and A. Lanzara, *Science* **336**, 1137 (2012).
- [19] W. Zhang, C. L. Smallwood, C. Jozwiak, T. L. Miller, Y. Yoshida, H. Eisaki, D.-H. Lee, and A. Lanzara, *Phys. Rev. B* **88**, 245132 (2013).
- [20] C. L. Smallwood, W. Zhang, T. L. Miller, C. Jozwiak, H. Eisaki, D.-H. Lee, and A. Lanzara, *Phys. Rev. B* **89**, 115126 (2014).
- [21] P. Kusar, V. V. Kabanov, J. Demsar, T. Mertelj, S. Sugai, and D. Mihailovic, *Phys. Rev. Lett.* **101**, 227001 (2008).
- [22] C. Giannetti, G. Coslovich, F. Cilento, G. Ferrini, H. Eisaki, N. Kaneko, M. Greven, and F. Parmigiani, *Phys. Rev. B* **79**, 224502 (2009).
- [23] C. Giannetti, M. Capone, D. Fausti, M. Fabrizio, F. Parmigiani, and D. Mihailovic, *Advances in Physics* **65**, 58 (2016).
- [24] A. Damascelli, Z. Hussain, and Z.-X. Shen, *Rev. Mod. Phys.* **75**, 473 (2003).
- [25] M. Sentef, A. F. Kemper, B. Moritz, J. K. Freericks, Z.-X. Shen, and T. P. Devereaux, *Phys. Rev. X* **3**, 041033 (2013).
- [26] A. Kemper, M. Sentef, B. Moritz, T. Devereaux, and J. Freericks, arXiv:1609.00087.
- [27] M. R. Norman, M. Randeria, H. Ding, and J. C. Campuzano, *Phys. Rev. B* **57**, R11093 (1998).
- [28] Y. Ishida, T. Saitoh, T. Mochiku, K. Nakane, T. and Hirata, and S. Shin, *Sci Rep* **6**, 18747 (2016).
- [29] H. Ding, M. R. Norman, J. C. Campuzano, M. Randeria, A. F. Bellman, T. Yokoya, T. Takahashi, T. Mochiku, and K. Kadowaki, *Phys. Rev. B* **54**, R9678 (1996).
- [30] M. R. Norman, H. Ding, M. Randeria, J. C. Campuzano, T. Yokoya, T. Takeuchi, T. Takahashi, T. Mochiku, K. Kadowaki, P. Guptasarma, and D. G. Hinks, *Nature* **392**, 157 (1998).
- [31] J. Graf, C. Jozwiak, C. L. Smallwood, H. Eisaki, R. A. Kaindl, D.-H. Lee, and A. Lanzara, *Nat Phys* **7**, 805 (2011).
- [32] H. Matsui, T. Sato, T. Takahashi, S.-C. Wang, H.-B. Yang, H. Ding, T. Fujii, T. Watanabe, and A. Matsuda, *Phys. Rev. Lett.* **90**, 217002 (2003).
- [33] T. Hanaguri, Y. Kohsaka, M. Ono, M. Maltseva, P. Coleman, I. Yamada, M. Azuma, M. Takano, K. Ohishi, and H. Takagi, *Science* **323**, 923 (2009).

- [34] J. P. Hinton, E. Thewalt, Z. Alpichshev, F. Mahmood, J. D. Koralek, M. K. Chan, M. J. Veit, C. J. Dorow, N. Bari, A. F. Kemper, D. A. Bonn, W. N. Hardy, R. Liang, N. Gedik, M. Greven, A. Lanzara, and J. Orenstein, *Scientific Reports* **6**, 23610 (2016).
- [35] S. Dal Conte, L. Vidmar, D. Golez, M. Mierzejewski, G. Soavi, S. Peli, F. Banfi, G. Ferrini, R. Comin, B. M. Ludbrook, L. Chauviere, N. D. Zhigadlo, H. Eisaki, M. Greven, S. Lupi, A. Damascelli, D. Brida, M. Capone, J. Bonca, G. Cerullo, and C. Giannetti, *Nat Phys.* **11**, 421 (2015).
- [36] J. D. Rameau, A. F. Kemper, M. A. Sentef, J. K. Freericks, I. Avigo, M. Ligges, L. Rettig, Y. Yoshida, H. Eisaki, J. Schneeloch, R. D. Zhong, Z. J. Xu, P. D. Gu, G. and D. Johnson, and U. Bovensiepen, *Nature Commun.* **7**, 13761 (2016).
- [37] R. D. Averitt, G. Rodriguez, A. I. Lobad, J. L. W. Siders, S. A. Trugman, and A. J. Taylor, *Phys. Rev. B* **63**, 140502 (2001).
- [38] R. A. Kaindl, M. A. Carnahan, D. S. Chemla, S. Oh, and J. N. Eckstein, *Phys. Rev. B* **72**, 060510 (2005).
- [39] Z. Zhang, C. Piovera, E. Papalazarou, M. Marsi, M. d'Astuto, C. J. van der Beek, A. Taleb-Ibrahimi, and L. Perfetti, arxiv:1703.07860v1.
- [40] S.-L. Yang, J. A. Sobota, D. Leuenberger, Y. He, M. Hashimoto, D. H. Lu, H. Eisaki, P. S. Kirchmann, and Z.-X. Shen, *Phys. Rev. Lett.* **114**, 247001 (2015).
- [41] J. A. Sobota, S.-L. Yang, D. Leuenberger, A. F. Kemper, J. G. Analytis, I. R. Fisher, P. S. Kirchmann, T. P. Devereaux, and Z.-X. Shen, *Phys. Rev. Lett.* **113**, 157401 (2014).
- [42] M. Tinkham, *Introduction to Superconductivity* (McGraw-Hill, Inc., 1996).
- [43] J. E. Hoffman, K. McElroy, D.-H. Lee, K. M. Lang, H. Eisaki, S. Uchida, and J. C. Davis, *Science* **297**, 1148 (2002).